Journal of Hazardous Materials 194 (2011) 109–118

Contents lists available at ScienceDirect

Journal of Hazardous Materials

journal homepage: www.elsevier.com/locate/jhazmat

Solar photoelectro-Fenton degradation of the herbicide 4-chloro-2-methylphenoxyacetic acid optimized by response surface methodology

Sergi Garcia-Segura [a], Lucio Cesar Almeida [b], Nerilso Bocchi [b], Enric Brillas [a,*]

[a] Laboratori d'Electroquímica dels Materials i del Medi Ambient, Departament de Química Física, Facultat de Química, Universitat de Barcelona, Martí i Franquès 1-11, 08028 Barcelona, Spain

[b] Laboratório de Pesquisas em Eletroquímica, Departamento de Química, Universidade Federal de São Carlos, C.P. 676, 13560-970 São Carlos – SP, Brazil

ARTICLE INFO

Article history:
Received 11 May 2011
Received in revised form 30 June 2011
Accepted 21 July 2011
Available online 5 August 2011

Keywords:
Herbicides
Solar photoelectro-Fenton
Central composite rotatable design
Response surface methodology
Oxidation products

ABSTRACT

A central composite rotatable design and response surface methodology (RSM) were used to optimize the experimental variables of the solar photoelectro-Fenton (SPEF) treatment of the herbicide 4-chloro-2-methylphenoxyacetic acid (MCPA). The experiments were made with a flow plant containing a Pt/air-diffusion reactor coupled to a solar compound parabolic collector (CPC) under recirculation of 10 L of 186 mg L^{-1} MCPA solutions in 0.05 M Na_2SO_4 at a liquid flow rate of 180 L h^{-1} with an average UV irradiation intensity of about 32 W m^{-2}. The optimum variables found for the SPEF process were 5.0 A, 1.0 mM Fe^{2+} and pH 3.0 after 120 min of electrolysis. Under these conditions, 75% of mineralization with 71% of current efficiency and 87.7 kWh kg^{-1} TOC of energy consumption were obtained. MCPA decayed under the attack of generated hydroxyl radicals following a pseudo-first-order kinetics. Hydroxyl radicals also destroyed 4-chloro-2-methylphenol, methylhydroquinone and methyl-*p*-benzoquinone detected as aromatic by-products. Glycolic, maleic, fumaric, malic, succinic, tartronic, oxalic and formic acids were identified as generated carboxylic acids, which form Fe(III) complexes that are quickly photodecarboxylated by the UV irradiation of sunlight at the CPC photoreactor. A reaction sequence for the SPEF degradation of MCPA was proposed.

1. Introduction

Several electrochemical treatments have been recently proposed for the decontamination of wastewaters containing inorganic [1,2] and organic pollutants [3–8]. Among them, electrochemical advanced oxidation processes based on Fenton chemistry such as electro-Fenton (EF) and photoelectro-Fenton (PEF) are being developed because they generate oxidant hydroxyl radical (•OH) for an effective mineralization of toxic organics to CO_2, water and inorganic ions [3,5,9]. In these techniques, H_2O_2 is supplied to an acidic solution by the two-electron reduction of O_2 gas from reaction (1), which is efficiently produced at carbonaceous cathodes like carbon felt [10–17], activated carbon fiber [18], carbon-polytetrafluoroethylene (PTFE) [3,8,12,19] and carbon nanotubes-PTFE [20–22] gas (O_2 or air) diffusion and boron-doped diamond (BDD) [23].

$$O_{2(g)} + 2H^+ + 2e^- \rightarrow H_2O_2 \quad (1)$$

The oxidizing power of electrogenerated H_2O_2 is then enhanced by adding small amounts of Fe^{2+} to produce Fe^{3+} and •OH in the bulk from Fenton reaction (2) [24]:

$$Fe^{2+} + H_2O_2 + H^+ \rightarrow Fe^{3+} + {}^{\bullet}OH + H_2O \quad (2)$$

The catalytic reaction (2) is propagated from Fe^{2+} regeneration, primordially by Fe^{3+} reduction at the cathode [5,11], allowing the dehydrogenation or hydroxylation of organics by non-selective attack of •OH until mineralization. When an one-compartment cell is utilized, organics can also be degraded by adsorbed hydroxyl radical (M(•OH)) formed as intermediate of water oxidation to O_2 on the anode M from reaction (3) [6,25]:

$$M(H_2O) \rightarrow M({}^{\bullet}OH) + H^+ + e^- \quad (3)$$

The BDD anode is usually preferred for wastewater remediation since it provides BDD(•OH) radicals with higher oxidizing power than those of other anodes due to its higher O_2-overpotential [6,26,27]. Nevertheless, the Pt anode yielding less potent Pt(•OH) radicals is widely used since it allows more inexpensive treatments by the lower cell potential applied [6,8,9,28].

The irradiation of the contaminated solution with UVA light (λ_{max} = 360 nm) in PEF accelerates the degradation of pollutants in

* Corresponding author. Tel.: +34 934021223; fax: +34 934021231.
E-mail address: brillas@ub.edu (E. Brillas).

0304-3894/$ – see front matter © 2011 Elsevier B.V. All rights reserved.
doi:10.1016/j.jhazmat.2011.07.089

EF, since it promotes the photodecomposition of Fe(III) complexes with generated by-products like carboxylic acids from reaction (4) and the enhancement of Fe^{2+} regeneration and $^{\bullet}OH$ production from the photolytic reaction (5) [5,9,10,18–21,29,30]:

$$Fe(OOCR)^{2+} + h\nu \rightarrow Fe^{2+} + CO_2 + R^{\bullet} \quad (4)$$

$$Fe(OH)^{2+} + h\nu \rightarrow Fe^{2+} + {}^{\bullet}OH \quad (5)$$

In our laboratory, we are exploring the alternative use of sunlight ($\lambda > 300$ nm) as an inexpensive and renewable energy source in the solar photoelectro-Fenton (SPEF) process. The use of solar light is expected to improve the performance of UVA lamps since photons in the UV region range of 300–400 nm, as well as in the visible region ranges of 400–450 nm [31] and 400–650 nm [32], but with much less quantum yield, can be absorbed for reactions (4) and (5), respectively. SPEF has been shown to mineralize some aromatic pollutants like cresols [3], the pharmaceutical paracetamol [8] and the azo dye Acid Yellow 36 [33]. However, more research efforts are required to know the degradation ability of this method on other kinds of pollutants to assess its possible application to industrial scale. In this way, we have studied the SPEF process of the herbicide 4-chloro-2-methylphenoxyacetic acid (MCPA), belonging to the family of phenoxyacetic acids, which are considered highly carcinogenic [34]. MCPA was chosen because it has been detected in natural and drinking waters with contamination levels up to 0.4 $\mu g\,L^{-1}$ [35,36], due to its widespread use in the selective control of perennial crops, grasslands and lawns [19,27]. At the pH of most soils the anionic form of this herbicide predominates allowing its leaching and the contamination of aquifers associated with its use [37].

This paper reports the SPEF degradation of 186 $mg\,L^{-1}$ MCPA solutions using a 10 L solar flow plant containing a Pt/air-diffusion cell coupled to a compound parabolic collector (CPC) under batch recirculation mode. The optimum experimental variables for this process have been determined with a central composite rotatable design (CCRD) coupled to response surface methodology (RSM) [38,39]. This statistical tool has been recently applied to the Fenton [40–42], photo-Fenton [42,43], solar photo-Fenton [44–47], peroxi-coagulation [22], EF [48,49] and SPEF [8] treatments of some organic compounds. The major advantage of RSM is that includes interactive effects among the variables to describe their complete influence on the process by means of a minimum number of assays [50]. The experiments were performed taking the current, Fe^{2+} content and pH as independent variables and using the analysis of variance (ANOVA) to validate the mathematical models developed [39]. The MCPA decay and the evolution of its by-products were determined by chromatographic techniques and a reaction sequence for MCPA degradation was proposed.

2. Experimental

2.1. Chemicals

MCPA, 4-chloro-2-methylphenol, methylhydroquinone and methyl-*p*-benzoquinone were reagent grade from Merck and Sigma–Aldrich. All carboxylic acids were analytical grade from Panreac and Avocado. Heptahydrated ferrous sulphate and anhydrous sodium sulphate were analytical grade from Fluka. The MCPA solutions were prepared with deionized water and their pH was adjusted with analytical grade sulphuric acid from Merck. Organic solvents and other chemicals employed were either HPLC or analytical grade from Merck, Fluka and Sigma–Aldrich.

2.2. Apparatus and analytical procedures

The solution pH was measured with a Crison GLP 22 pH-meter. Before analysis, aliquots of 7 mL withdrawn from electrolyzed solutions were neutralized at pH 7–8 to stop the degradation process and filtered with 0.45 μm PTFE filters from Whatman. The mineralization process was monitored from the total organic carbon (TOC) abatement of solutions using a Shimadzu VCSN analyzer. From this data and assuming the overall mineralization of MCPA to CO_2 and Cl^- ion via reaction (6):

$$C_9H_9ClO_3 + 15H_2O \rightarrow 9CO_2 + Cl^- + 39H^+ + 38e^- \quad (6)$$

the mineralization current efficiency (MCE) was estimated from Eq. (7) [30,33]:

$$\%\,MCE = \frac{nFV_s\Delta(TOC)_{exp}}{4.32 \times 10^7 mIt} \times 100 \quad (7)$$

where n is the number of electrons consumed per MCPA molecule (38), F is the Faraday constant (96487 $C\,mol^{-1}$), V_s is the solution volume (L), $\Delta(TOC)_{exp}$ is the experimental solution TOC decay ($mg\,L^{-1}$), 4.32×10^7 is a conversion factor ($3600\,s\,h^{-1} \times 12{,}000\,mg\,mol^{-1}$), m is the number of carbon atoms of MCPA (9 atoms), I is the applied current (A) and t is the electrolysis time (h). The energy consumption per unit TOC mass (EC) was calculated from Eq. (8) [5,33]:

$$EC\,(kWh\ kg^{-1}\,TOC) = \frac{1000\,E_{cell}It}{V_s\Delta(TOC)_{exp}} \quad (8)$$

where E_{cell} is the average cell potential (V) and 1000 is a conversion factor ($mg\,g^{-1}$).

The MCPA decay and the evolution of its aromatic intermediates were followed by reversed-phase HPLC using a Waters 600 LC fitted with a Spherisorb ODS2 5 μm, 150 mm × 4.6 mm, column at 35 °C, coupled with a Waters 996 photodiode array detector selected at λ of 230 nm for MCPA, 229 nm for 4-chloro-2-methylphenol, 269 nm for methylhydroquinone and 248 nm for methyl-*p*-benzoquinone. Carboxylic acids were detected by ion-exclusion HPLC using the above LC fitted with a Bio-Rad Aminex HPX 87H, 300 mm × 7.8 mm, column at 35 °C and the photodiode array detector selected at λ = 210 nm. The mobile phase was 70:30 (v/v) acetonitrile/phosphate buffer (pH 3.5) at 0.3 mL min^{-1} for reversed-phase HPLC and 4 mM H_2SO_4 at 0.6 mL min^{-1} for ion-exclusion HPLC. The Cl^- concentration was determined by ionic chromatography with a Shimadzu 10 Avp HPLC fitted with a Shim-Pack IC-A1S, 100 mm × 4.6 mm, anion column at 40 °C, coupled with a Shimadzu CDD 10 Avp conductivity detector, using a 2.4 mM tris(hydroxymethyl)-aminomethane and 2.5 mM phthalic acid solution of pH 4.0 at 1.0 mL min^{-1} as mobile phase.

2.3. Solar flow plant

Fig. 1 shows the sketches of the solar flow plant and the electrolytic filter-press cell used for the SPEF degradation of 10 L of 186 $mg\,L^{-1}$ MCPA solutions in 0.05 M Na_2SO_4. The solution introduced in the reservoir was recirculated by a peristaltic pump at 180 L h^{-1} adjusted by a rotameter and thermostated at 35 °C by two heat exchangers. The cell contained a Pt sheet of 99.99% purity from SEMPSA and a carbon-PTFE air-diffusion electrode from E-TEK for H_2O_2 electrogeneration from reaction (1). Both electrodes of 10 cm × 10 cm in dimension were separated 1.2 cm by a PVC liquid compartment with a central window of 9.5 cm × 9.5 cm (90.3 cm^2). The inner face of the cathode was in contact with a PVC gas chamber fed with compressed air at 4.5 L min^{-1} regulated with a back-pressure gauge. The current to the Pt/air-diffusion cell was supplied by a Grelco GDL3020 power supply, which directly displayed the applied potential. The solar CPC photoreactor with a concentration

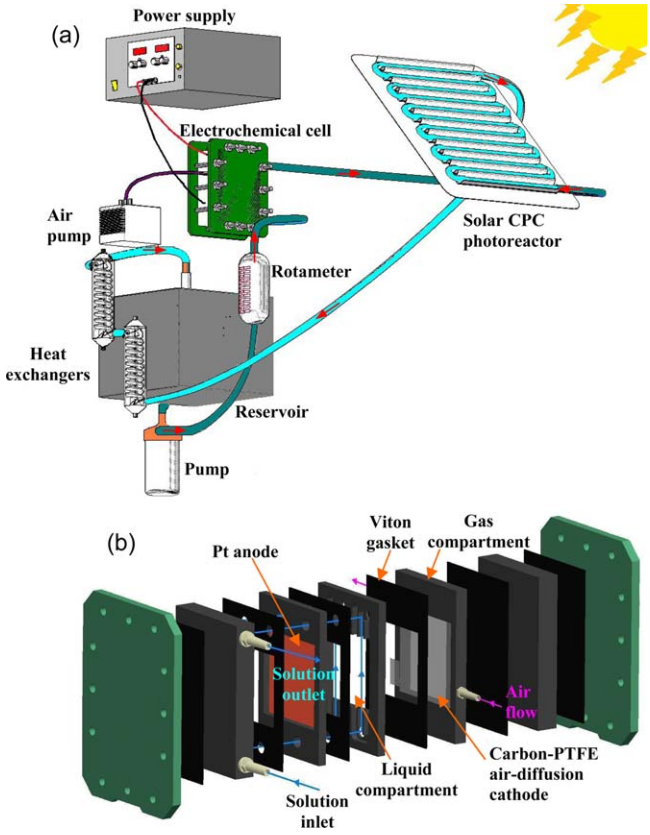

Fig. 1. Sketches of the: (a) 10 L recirculation flow plant used for the solar photelectro-Fenton (SPEF) treatment of 4-chloro-2-methylphenoxyacetic acid (MCPA) and (b) one-compartment Pt/air-diffusion filter-press cell of 90.3 cm^2 electrode area. The compound parabolic collector (CPC) contained 1.57 L of solution and was directly illuminated with sunlight.

factor of 1 and 0.4 m^2 area contained 12 borosilicate-glass tubes of 50.5 cm length × 1.82 cm inner diameter (irradiated volume 1.57 L), mounted in an aluminium frame on a platform tilted 41° to better collect the direct sun rays in our laboratory of Barcelona (latitude: 41°21′N, longitude: 2°10′E). Solar trials were performed in sunny and clear days during summer 2010 and the UV irradiation intensity (300–400 nm) was measured with a Kipp & Zonen CUV 5 radiometer.

2.4. Experimental design and response surface methodology

To optimize the SPEF degradation of MCPA by CCRD and RSM, the current, Fe^{2+} concentration and pH were selected as independent variables, whereas TOC, MCE and EC were taken as responses. The CCRD considered eight factorial points, six axial points and three central points [38,39], ranging the current from 1.6 to 8.4 A, Fe^{2+} content from 0.41 to 2.09 mM and pH from 1.32 to 4.68. Five levels were chosen for each independent variable (see Table 1), coded as follows [50]:

$$x_i = \frac{X_i - X_{i0}}{\Delta X_i} \quad (9)$$

where x_i, X_i, X_{i0}, and ΔX_i are the coded level of the ith independent variable, the real value of the ith independent variable, the real value of the ith independent variable in the central point and the half of the difference between the upper and lower values of the ith independent variable, respectively.

The correlations between the independent variables and responses were obtained by the following second-order model with a least-squares method [50]:

$$Y = \beta_0 + \sum_{i=1}^{k} \beta_i x_i + \sum_{i=1}^{k} \beta_{ii} x_i^2 + \sum_{i=1}^{k} \sum_{i \neq j=1}^{k} \beta_{ij} x_i x_j + \varepsilon \quad (10)$$

where Y is the response, β_0 is a constant coefficient, β_i, β_{ii}, and β_{ij} are the coefficients for the linear, quadratic and interaction effects,

Table 1
Coded levels and real values for the central composite rotatable design used for the RSM analysis of the SPEF treatment of 186 mg L^{-1} 4-chloro-2-methylphenoxyacetic acid solutions in 0.05 M Na_2SO_4 at 35 °C with a 10 L flow plant containing a Pt/air-diffusion cell coupled to a solar CPC photoreactor.

Run	Coded levels			Real values			Observed responses			UV intensity[g]/W m^{-2}
	x_1	x_2	x_3	X_1[a]	X_2[b]	X_3[c]	TOC_{120}[d]/mg L^{-1}	% MCE_{120}[e]	EC_{120}[f]/kWh kg^{-1} TOC	
1	−1	−1	−1	3.0	0.75	2.00	25.2	78.9	84.5	32.1
2	1	−1	−1	7.0	0.75	2.00	20.7	50.2	156.8	30.3
3	−1	1	−1	3.0	1.75	2.00	78.7	22.5	247.2	31.4
4	1	1	−1	7.0	1.75	2.00	60.5	25.0	268.7	30.7
5	−1	−1	1	3.0	0.75	4.00	30.1	73.7	92.6	33.7
6	1	−1	1	7.0	0.75	4.00	27.1	46.1	196.0	31.8
7	−1	1	1	3.0	1.75	4.00	33.6	70.0	86.0	31.5
8	1	1	1	7.0	1.75	4.00	53.5	29.4	273.6	32.1
9	−1.68	0	0	1.6	1.25	3.00	40.9	80.1	46.3	32.8
10	+1.68	0	0	8.4	1.25	3.00	20.8	44.2	212.6	32.4
11	0	−1.68	0	5.0	0.41	3.00	24.0	60.1	113.7	30.8
12	0	+1.68	0	5.0	2.09	3.00	60.1	31.6	194.5	31.0
13	0	0	−1.68	5.0	1.25	1.32	36.0	50.6	136.3	30.0
14	0	0	+1.68	5.0	1.25	4.68	55.4	35.3	217.2	30.2
15	0	0	0	5.0	1.25	3.00	30.6	54.9	138.3	31.3
16	0	0	0	5.0	1.25	3.00	31.1	54.5	138.8	30.6
17	0	0	0	5.0	1.25	3.00	31.0	54.6	137.9	32.3

[a] Current (A).
[b] Fe^{2+} concentration (mM).
[c] pH.
[d] Total organic carbon at 120 min.
[e] Mineralization current efficiency at 120 min.
[f] Energy consumption per unit TOC mass at 120 min.
[g] Average UV irradiation intensity supplied by sunlight for 120 min.

respectively, x_i and x_j are the coded levels for the independent variables, k is the number of independent variables and ε is the random error.

The three replicates in the central point (runs 15–17) were performed to estimate the pure error. The experiments were randomly carried out to minimize the effect of unexplained variability on the observed responses due to systematic errors [51]. The response surfaces were generated by a StatSoft STATISTICA v6 program and the quadratic models were validated by ANOVA, checking their fit quality by the determination coefficient R^2 and their statistical significances by the F-test [38,50].

3. Results and discussion

3.1. SPEF degradation of MCPA solutions

The MCPA solutions were degraded in the solar flow plant from noon to 16 h as maximum. The initial colorless solutions consecutively changed to yellow, orange and yellow color, becoming colorless again in 60–80 min. This phenomenon suggests the formation of colored conjugated intermediates, like benzoquinonic derivatives, that are progressively removed by •OH [5,33]. The solution pH decreased during electrolysis owing to the formation of acidic derivatives like carboxylic acids and for this reason, it was continuously regulated to its initial value by adding small volumes of 1.0 M NaOH.

Fig. 2a exemplifies the TOC abatement for the SPEF treatment of MCPA solutions under different conditions. As can be seen, partial mineralization of the herbicide was always found at 240 min of electrolysis, although the quicker degradations up to 79–83% TOC reduction were obtained at 120 min. Fig. 2b and c shows that the most potent trials possess maximum MCE values, related to minimum EC values, between 60 and 120 min of treatment. The time of 120 min was then taken to optimize the independent variables from CCRD. Table 1 summarizes the observed responses thus obtained for all coded levels. The last column of Table 1 evidences that a similar average UV irradiation intensity from 30.0 to 33.7 W m^{-2} was supplied to the solar CPC photoreactor during 120 min of electrolysis.

3.2. Influence of experimental variables on the SPEF process

The observed responses of Table 1 were analyzed with a multiple linear-regression model and least-squares method [38] to generate the following equations for the adjusted second-order models of TOC_{120}, MCE_{120} and EC_{120} (at 95% confidence level):

$$TOC_{120} = 25.71 - 13.40x_1 + 5.49x_2 + 5.36x_3 + 8.46x_1^2 + 4.15x_2^2 + 2.00x_3^2 + 4.56_2x_3 \quad (11)$$

$$MCE_{120} = 69.94 - 11.5x_1 - 6.06x_2 - 6.03x_3 - 3.93x_1^2 - 3.56x_2^2 - 1.54x_3^2 + 4.13x_1x_3 - 5.85x_2x_3 \quad (12)$$

$$EC_{120} = 90.31 + 51.28x_1 + 10.94x_2 + 16.85x_3 + 14.94x_1^2 + 8.38x_2^2 + 5.91x_3^2 + 17.94x_2x_3 \quad (13)$$

where x_1, x_2 and x_3 denote the current, initial Fe^{2+} concentration and pH, respectively.

Fig. 3 illustrates several response surfaces from these quadratic models. The negative coefficient of x_1 in Eq. (11) indicates, in principle, a quick TOC_{120} abatement with increasing current, as shown in Fig. 3a in the range of 1.6–7.0 A, where 80% of TOC_{120} can be removed. This behavior is explained by the higher •OH production from Fenton reaction (2) as result of the greater H_2O_2 generation by reaction (1) and Fe^{2+} regeneration from Fe^{3+} reduction at the cathode [3,5,33]. However, the response surface of Fig. 3a shows a negative influence on TOC_{120} decay for currents >7.0 A caused by the higher positive increase of the quadratic term $x_1{}^2$ in Eq. (11). This effect can be attributed to the enhancement of non-oxidizing reactions of •OH involving, for example, its dimerization by reaction (14) or its attack on H_2O_2 by reaction (15) [5,52], thus producing a decrease in organic events and TOC_{120} removal.

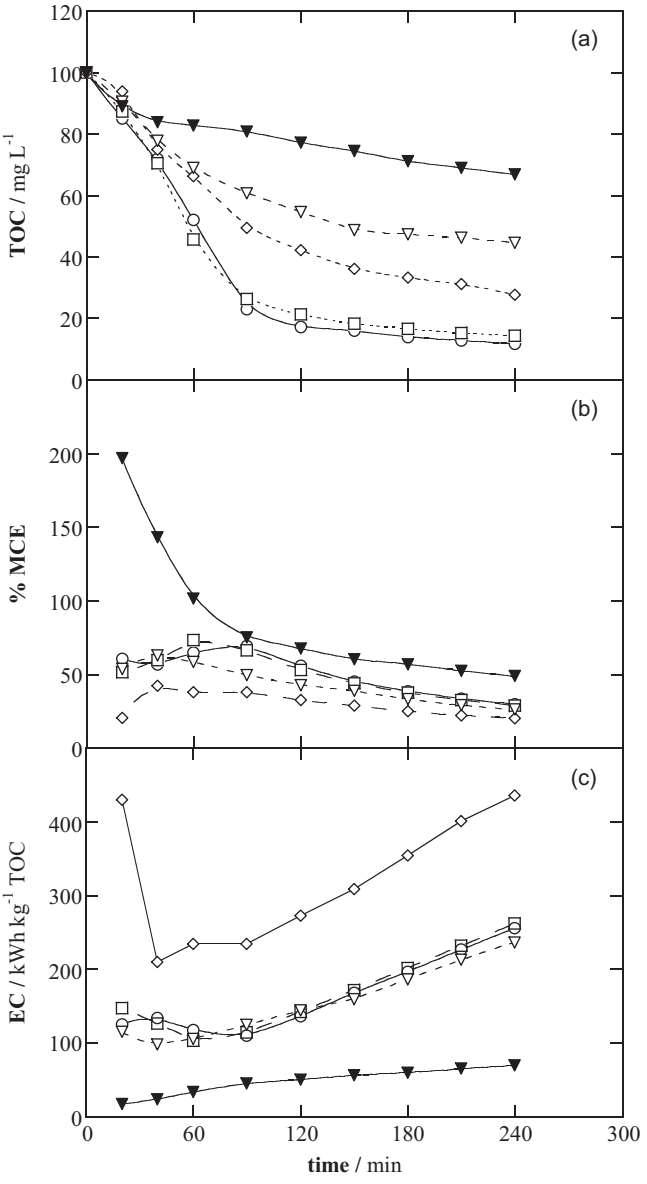

Fig. 2. Change of: (a) TOC, (b) mineralization current efficiency (MCE) and (c) energy consumption per unit TOC mass (EC) with electrolysis time for the SPEF treatment of 186 mg L^{-1} MCPA solutions in the solar flow plant. Experimental conditions: (□) 7.0 A, 0.75 mM Fe^{2+}, pH 2.0 (run 2), (○) 7.0 A, 0.75 mM Fe^{2+}, pH 4.0 (run 6), (▼) 1.6 A, 1.25 mM Fe^{2+}, pH 3.0 (run 9), (◊) 8.4 A, 1.25 mM Fe^{2+}, pH 3.0 (run 10) and (▽) 5.0 A, 2.09 mM Fe^{2+}, pH 3.0 (run 12).

$$^{\bullet}OH + {}^{\bullet}OH \rightarrow H_2O_2 \quad (14)$$

$$H_2O_2 + {}^{\bullet}OH \rightarrow HO_2{}^{\bullet} + H_2O \quad (15)$$

The influence of Fe^{2+} concentration on TOC_{120} decay was not so pronounced. Fig. 3a and b shows that maximum MCPA mineralization is achieved between 0.75 and 1.25 mM Fe^{2+}, whereas lower

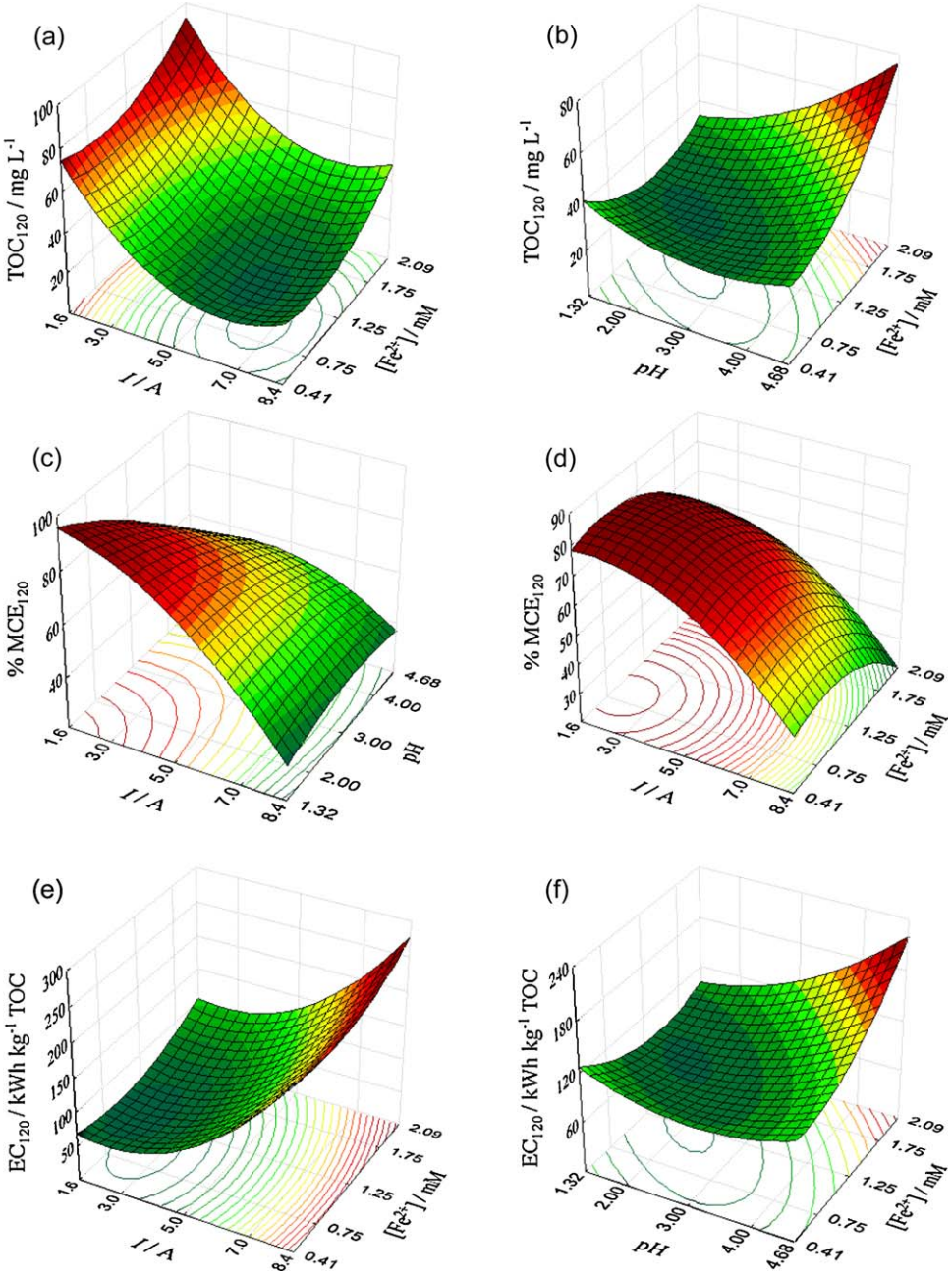

Fig. 3. Response surfaces generated from the central composite rotatable design after 120 min of SPEF treatment of 10 L of 186 mg L^{-1} MCPA solutions in the solar flow plant using Eqs. (11)–(13). (a) TOC_{120} for Fe^{2+} concentration vs. current, (b) TOC_{120} for Fe^{2+} concentration vs. pH, (c) MCE_{120} for pH vs. current, (d) MCE_{120} for current vs. Fe^{2+} concentration, (e) EC_{120} for Fe^{2+} concentration vs. current and (f) EC_{120} for pH vs. Fe^{2+} concentration.

and higher Fe^{2+} concentrations progressively yield lower mineralization. The loss of TOC_{120} abatement for Fe^{2+} contents below 0.75 mM can be associated with the decrease in rate of Fenton reaction (2) by the smaller quantity of this ion, producing less oxidant •OH. In contrast, for Fe^{2+} concentrations >1.25 mM, the excess of this ion can react rapidly with •OH from reaction (16) [24], decreasing the quantity of this radical for organic oxidation and inhibiting the mineralization process.

$$Fe^{2+} + {}^{\bullet}OH \rightarrow Fe^{3+} + OH^{-} \quad (16)$$

Fig. 3b also evidences that the best pH for TOC_{120} removal is reached between 2.0 and 3.0, close to the optimum pH 2.8 for Fenton reaction (2) [24]. In this interval, nearly 80% of TOC_{120} is removed at 120 min, corroborating that organics are mainly oxidized by •OH.

When MCE_{120} is considered, the fact that most coefficients of Eq. (12) are negative indicates a dramatic decay of this parameter with increasing all the independent variables, as can be seen in Fig. 3c and d. The strong decrease in MCE_{120} as current rises (see Fig. 3c) may seem contradictory to the larger mineralization reached because TOC_{120} undergoes a gradual and rapid abatement (see Fig. 3a), at least until 7.0 A, by the greater •OH production from Fenton reaction (2). This phenomenon corroborates the role of the waste reactions (14) and (15) to decrease the amount of this radical for destroying the organic pollutants. Fig. 3c shows a maximum MCE_{120} of 95% for 1.6 A and pH 1.32, which is reduced for the same current when pH varies from 3.00 to 4.68 due to the deceleration of Fenton reaction (2) yielding less •OH. Fig. 3d also evidences that maximum MCE_{120} near 80% is obtained for the lower currents and Fe^{2+} concentrations between 0.41 and 1.25 mM. At

higher Fe^{2+}content, this parameter gradually decays because •OH is consumed by the excess of Fe^{2+} via reaction (16).

On the other hand, Fig. 3e shows an increase in EC_{120} when current rises from 1.6 to 8.4 A, whereas Fig. 3e and f evidences that this response presents its lower values from 0.75 to 1.25 mM Fe^{2+}, consistent with the behavior of TOC_{120} surfaces (see Fig. 3a and b). For currents between 1.6 and 5.0 A and 1.0 mM Fe^{2+}, energy consumptions of 110 kWh kg^{-1} TOC are obtained, which increase to 280 kWh kg^{-1} TOC for the higher currents, regardless of Fe^{2+} concentration. Fig. 3f also shows a minimum region for EC_{120} at pH near 3.0 when the oxidation process becomes more potent for the greater •OH production from Fenton reaction (2).

3.3. Validation of the quadratic models developed

To assess the adequacy of the quadratic models of Eqs. (11)–(13) to describe the experimental results, ANOVA was applied. For this, the Fisher distribution (*F*-test) was used to statistically validate the significance of regressions and the lack of fit for these models. The significance of the three models developed was then assessed from the ratio between the mean squares of the regression and residuals, whereas the adjustment of the models was evaluated by the ratio between the mean squares of lack of fit and pure error. The *F*-ratio calculated for the regressions was 5.416 for TOC_{120}, 13.646 for EC_{120} and 3.728 for MCE_{120}, higher than the tabulated value (3.293) for 95% confidence level, confirming that the models are statistically significant [51]. Moreover, the *F*-ratio obtained for the lack of fit was lower than the tabulated value (19.296) for 95% confidence level, being 5.597 for TOC_{120}, 16.817 for EC_{120} and 7.678 for MCE_{120}, indicating that the models are satisfactory without evidencing a lack of fit [50,51]. Fig. 4a exemplifies the plot of the residual vs. predicted values for EC_{120}, showing that residuals are randomly distributed around the mean due to the good agreement of the model and discarding the existence of systematic errors. Fig. 4b depicts the good linear correlation found between the predicted and observed values for EC_{120}, with a determination coefficient $R^2 = 0.946$. Similar residual-predicted and predicted-observed plots for TOC_{120} and MCE_{120} were found, with R^2 values of 0.875 and 0.830, for the respective linear predicted-observed correlations. The fact that determination coefficients are close to unity also corroborates the statistical significance of the three quadratic models developed.

3.4. Optimization of the SPEF degradation of MCPA

From the response surfaces generated using RSM, the optimum conditions for the SPEF degradation of 186 mg L^{-1} MCPA solutions were established considering that they would provide higher TOC removal with good current efficiency and lower energy consumption. Our results indicate that the optimum MCPA mineralization takes place at pH 3.0 and Fe^{2+} concentration between 0.75 and 1.25 mM, where acceptable MCE_{120} and EC_{120} values are found at near 5.0 A. Consequently, 5.0 A, 1.0 mM Fe^{2+} and pH 3.0 were selected as the best operational conditions. This Fe^{2+} content was chosen because it is the central value within 0.75 and 1.25 mM Fe^{2+}.

Fig. 5 illustrates the evolution of TOC, EC and MCE for the 186 mg L^{-1} MCPA solution in the solar flow plant under the optimum SPEF conditions. A gradual TOC reduction to 24.6 mg L^{-1} can be observed at 120 min of electrolysis, coincident with the predicted value of 25.0 mg L^{-1} from Eq. (11), whereas at 140 min a minimum TOC of 20 mg L^{-1} is already achieved. Moreover, MCE rises to 71% and EC decreases to 87.7 kWh kg^{-1} TOC (6.6 kWh m^{-3}) at 120 min, in good agreement with 72% and 85.0 kWh kg^{-1} TOC obtained from Eqs. (12) and (13), respectively. These results demonstrate the excellent description of the SPEF process by the quadratic models developed by RSM.

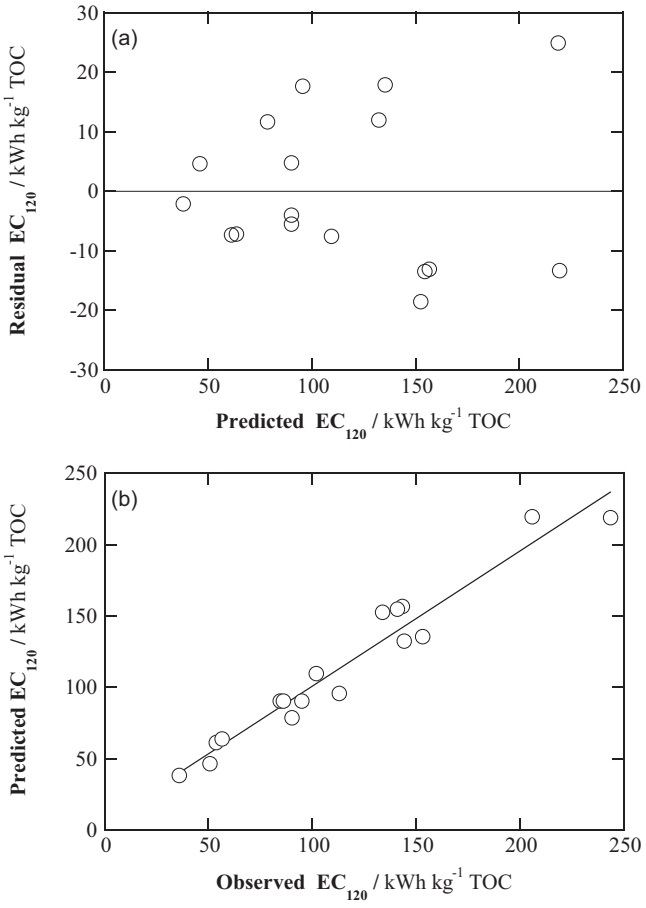

Fig. 4. (a) Residual-predicted and (b) predicted-observed plots for the energy consumption per unit TOC mass at 120 min of electrolysis found by response surface methodology (RSM) for the SPEF process of MCPA in the solar flow plant. Predicted values were calculated from Eq. (13) and residual values as the difference between the observed and predicted ones.

3.5. Decay kinetics for MCPA and identification and evolution of its by-products

The kinetics of the reaction between MCPA and generated •OH from Fenton reaction (2) induced by the photolytic reaction (5) was followed by reversed-phase HPLC where the herbicide displayed a well-defined peak at retention time (t_r) of 3.51 min. Direct photolysis of the herbicide was discarded because its content remained constant after 60 min of recirculating the initial solution through the solar flow plant without passing current by the electrochemical cell.

Fig. 6a shows that the 186 mg L^{-1} of MCPA disappear rapidly from the medium in 60 min under the optimized SPEF conditions, while its decay fits with the expected equation for a pseudo-first-order kinetics. From this analysis, a pseudo-first-order rate constant $k_1 = 1.25 \times 10^{-3}$ s^{-1} ($R^2 = 0.984$) is found. Since the second-order rate constant for the reaction between MCPA and •OH is $k_2 = 6.6 \times 10^9$ M^{-1} s^{-1} [53], one can infer that $k_1 = k_2$ [•OH] and hence, a constant •OH concentration ($=k_1/k_2$) of 1.9×10^{-13} M is produced in the SPEF system to attack the herbicide.

Aromatic intermediates like methylhydroquinone (t_r = 5.89 min), methyl-*p*-benzoquinone (t_r = 7.00 min) and 4-chloro-2-methylphenol (t_r = 8.10 min) were identified in the electrolyzed solutions by reversed-phase HPLC from comparison of their retention times and UV–vis spectra with pure compounds. Fig. 6b shows that these compounds are completely removed in 50–70 min, after reaching maxima of 0.64, 0.59 and 1.06 mg L^{-1},

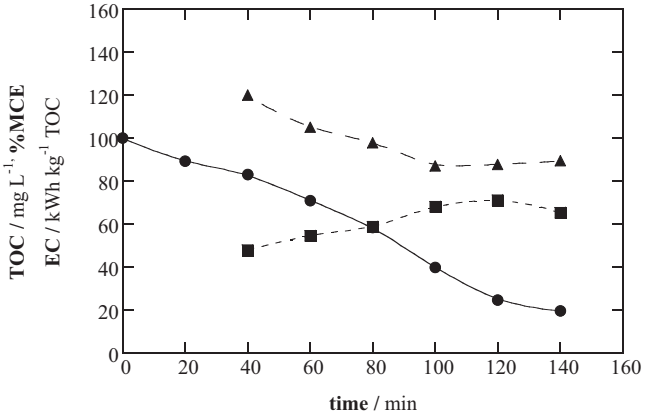

Fig. 5. Variation of: (●) TOC, (■) mineralization current efficiency and (▲) energy consumption per unit TOC mass with electrolysis time for the SPEF treatment of a 186 mg L^{-1} MCPA solution under the optimum conditions of 5 A, 1.00 mM Fe^{2+} and pH 3.0 found by RSM.

respectively. These by-products are then quickly formed and destroyed while MCPA is removed, indicating that they are also destroyed by generated •OH. This behavior confirms the fast disappearance of colored conjugated aromatics compounds formed during the SPEF process under the action of this radical, as stated above.

Ion-exclusion chromatograms of the electrolyzed solutions displayed peaks ascribed to oxalic (t_r = 6.98 min), tartronic (t_r = 7.96 min), maleic (t_r = 8.2 min), malic (t_r = 9.50 min), succinic (t_r = 11.7 min), glycolic (t_r = 13.0 min), formic (t_r = 13.7 min) and

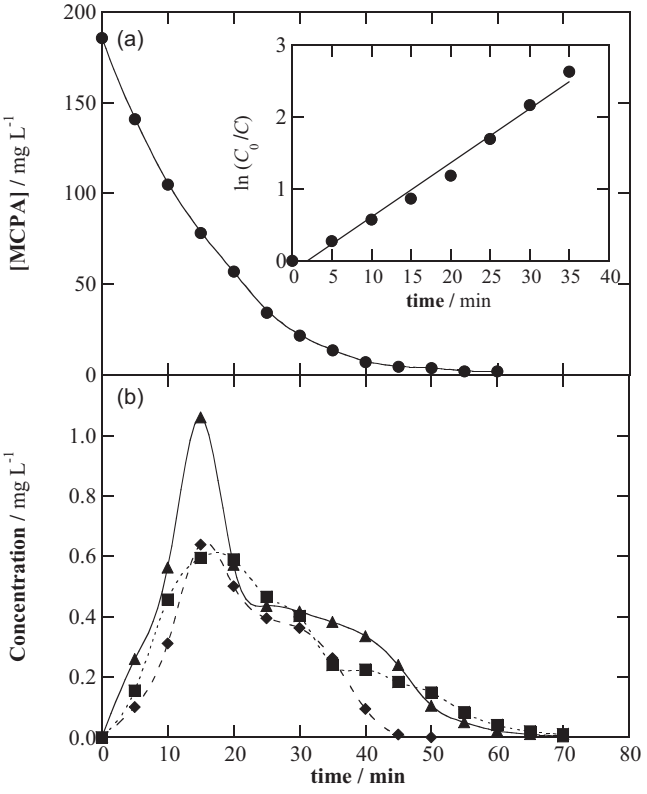

Fig. 6. (a) MCPA concentration decay during the optimized SPEF trial of Fig. 5. The inset panel presents the kinetic analysis considering a pseudo-first-order reaction for MCPA. (b) Evolution of the concentration of: (▲) 4-chloro-2-methylphenol, (♦) methylhydroquinone and (■) methyl-*p*-benzoquinone detected as aromatic by-products.

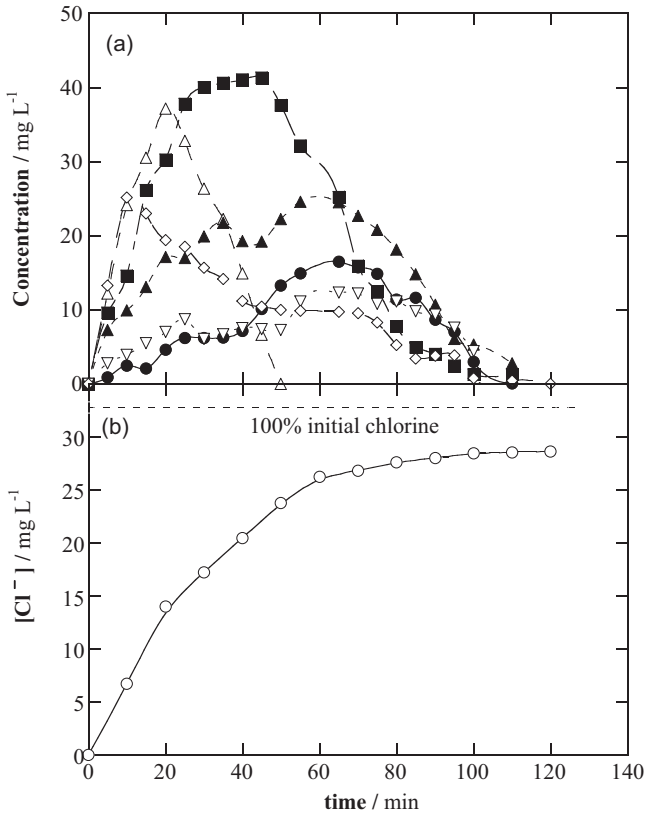

Fig. 7. (a) Evolution of the concentration of carboxylic acids: (▲) succinic, (△) malic, (■) tartronic, (◊) glycolic, (●) oxalic and (▽) formic acids during the experiment of Fig. 5. (b) Time-course of released chloride ion.

fumaric (t_r = 14.7 min) acids. Glycolic acid is expected to be generated when 4-chloro-2-methylphenol is produced, whereas maleic, fumaric, malic, succinic and tartronic acids can be formed from the cleavage of the benzenic ring of aromatic by-products [5,11,28]. Further oxidation of these acids yields oxalic and formic as ultimate acids that are directly mineralized to CO_2. In the experimental conditions tested, the Fe^{3+} ion generated from Fenton reaction (2) forms complexes with all these acids, which are practically not mineralized with •OH under EF conditions but quickly photodecarboxylated by UV light via reaction (4) [3,5,9,19,29,30,33]. The rapid removal of these compounds under the optimized SPEF conditions is presented in Fig. 7a. As can be seen, oxalic, formic, succinic, glycolic and tartronic acids are largely accumulated to 12, 12, 22, 25 and 41 mg L^{-1}, respectively, further being their Fe(III) complexes completely removed in 100–120 min. In contrast, malic acid attains a maximum of 37 mg L^{-1} and its Fe(III) complexes persist for shorter time, only 50 min. The evolution of maleic and fumaric acids is not shown in Fig. 7a because they are only accumulated up to 0.3 and 0.2 mg L^{-1}, respectively, disappearing the Fe(III)–maleate and Fe(III)–fumerate complexes in 110 min. These findings demonstrate the high power and effectiveness of UV light supplied by solar irradiation at the CPC photoreactor to rapidly remove the Fe(III)–carboxylate complexes enhancing the oxidation ability of the SPEF process.

The mineralization of MCPA is accompanied by the loss of its initial chlorine (32.8 mg L^{-1}) as Cl^- ion, as confirmed by ionic chromatography. Fig. 7b shows that this ion is continuously accumulated until 28.7 mg L^{-1} (88% of initial Cl) at 140 min of electrolysis. Since the released Cl^- ion is stable in a Pt/O_2 cell under PEF conditions [9,19], one can infer that 12% of initial Cl (4.1 mg L^{-1})

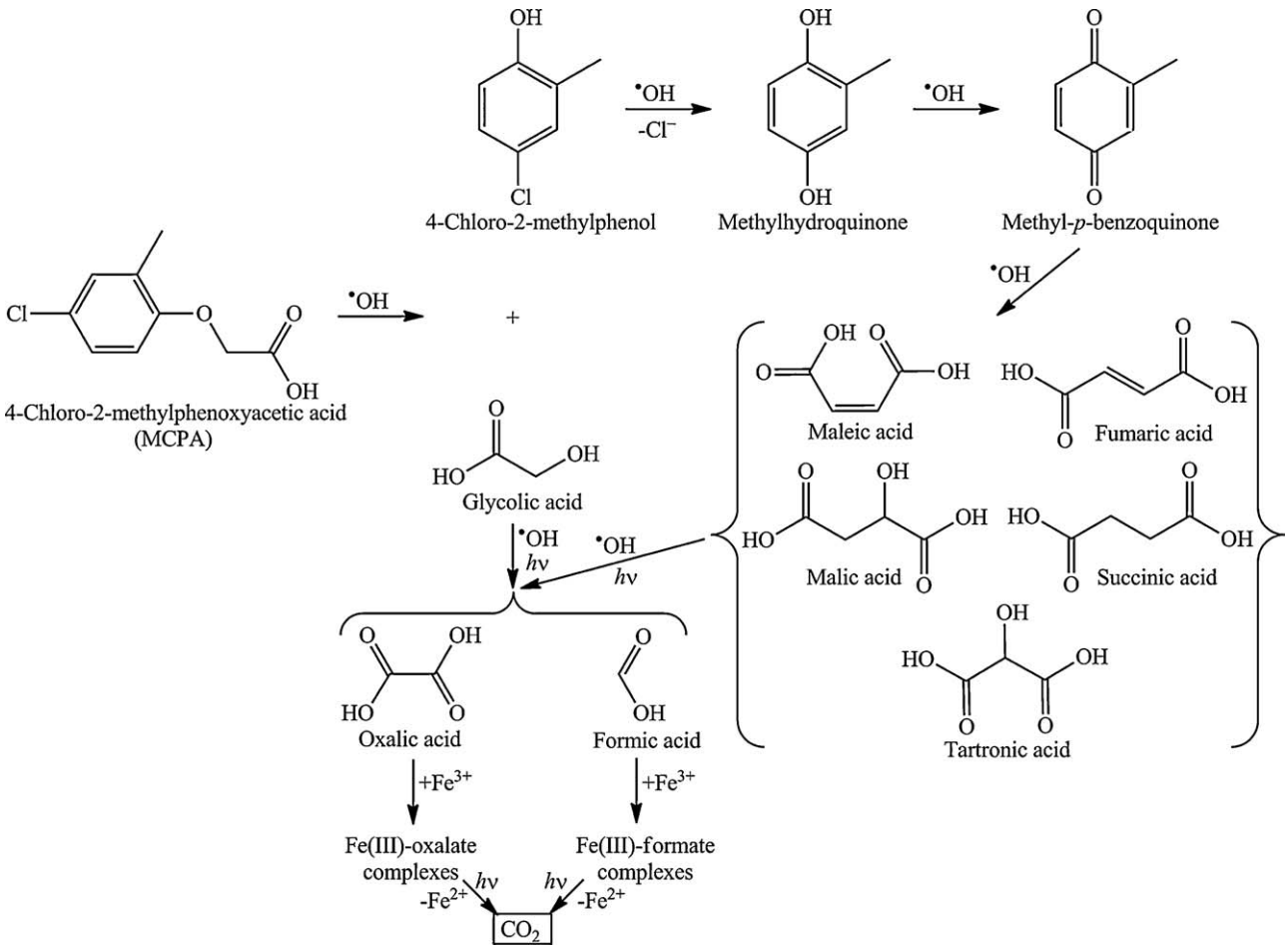

Fig. 8. Reaction sequence proposed for the SPEF degradation of MCPA.

is contained in stable chloroderivatives that remain in the final electrolyzed solution with 20 mg L^{-1} of TOC (see Fig. 5).

3.6. Reaction sequence for MCPA degradation

From the above detected by-products, a plausible reaction sequence for the SPEF degradation of MCPA is proposed in Fig. 8. The pathway assumes that aromatics are oxidized by •OH in the bulk, mainly generated from reactions (2) and (5), while the Fe(III)–carboxylate acids are slowly destroyed by this radical and quickly photodecomposed by UV irradiation of sunlight. For simplicity, only the photolysis of Fe(III)–oxalate and Fe(III)–formate complexes is depicted.

The process is initiated by the attack of •OH on the C(1)–O bond of MCPA giving 4-chloro-2-methylphenol and glycolic acid. Further hydroxylation of 4-chloro-2-methylphenol with dechlorination leads to Cl^- ion and methylhydroquinone, which is dehydrogenated to methyl-*p*-benzoquinone. Subsequent oxidation of this by-product yields a mixture of maleic, fumaric, malic, succinic and tartronic acids, which are converted into oxalic and formic acids. These two acids are also formed from the oxidation of the initially generated glycolic acid. Photodecarboxylation of Fe(III)–oxalate and Fe(III)–formate species finally yields CO_2 with Fe^{2+} regeneration [24,29]. Other unidentified and more persistent compounds including stable chloroderivatives are also produced, preventing the total mineralization of MCPA.

Note that MCPA degradation follows mainly the above pathway at least until 60 min of SPEF treatment while the majority of generated carboxylic acids are accumulated (see Fig. 7a). For example, while the MCPA solution treated at 20 min of electrolysis contains 89 mg L^{-1} TOC (see Fig. 5), the TOC corresponding to the herbicide, aromatic intermediates and carboxylic acids is 18, 1.1 and 39 mg L^{-1}, as deduced from Figs. 6a, b and 7a, respectively. That means that the generated carboxylic acids contribute to 44% of the solution TOC, indicating that they are the main by-products formed during the mineralization process.

4. Conclusions

A CCRD coupled with RSM allows describing adequately the behavior of the SPEF degradation of 186 mg L^{-1} MCPA solutions in a 10 L solar flow plant under recirculation batch mode. For the optimum conditions of 5 A, 1.0 mM Fe^{2+} and pH 3.0 at 120 min of electrolysis under an average UV irradiation of about 32 W m^{-2}, TOC was reduced by 75% with 71% of MCE and 87.7 kWh kg^{-1} TOC (6.6 kWh m^{-3}) of energy consumption. A TOC removal of 80% was reached at 140 min, with 88% of Cl^- ion released. The MCPA decay followed a pseudo-first-order kinetics, yielding 4-chloro-2-methylphenol and glycolic acid. Further oxidation of 4-chloro-2-methylphenol gives methylhydroquinone and methyl-*p*-benzoquinone. The cleavage of the benzene ring of latter aromatic leads to maleic, fumaric, malic, succinic and tartronic acids, which are subsequently transformed into the final oxalic and formic acids. While aromatics are mainly destroyed by •OH in the bulk, carboxylic acids form Fe(III) complexes that are quickly photolyzed by UV light of solar irradiation. Total MCPA mineralization was

prevented by the formation of other undetected and more persistent by-products.

Acknowledgements

The authors are grateful to MICINN (Ministerio de Ciencia e Innovación, Spain) for financial support through project CTQ 2010-16164/BQU, cofinanced with Feder funds. The grants awarded to S. Garcia-Segura by MEC (Ministerio de Educación y Ciencia, Spain) and L.C. Almedia by CNPq (Conselho Nacional de Desenvolvimento Científico e Tecnológico, Brazil) are acknowledged. The authors are also indebted to Sergio Garcia-Gallego, Marta Martínez and Ángel Romero for their help in the preparation of Fig. 1.

References

[1] L.H.S. Gasparotto, N. Bocchi, R.C. Rocha-Filho, S.R. Biaggio, Removal of Pb(II) from simulated wastewaters using a stainless steel wool cathode in a flow-through cell, J. Appl. Electrochem. 36 (2006) 677–683.
[2] L.C. Almeida, L.H.S. Gasparotto, N. Bocchi, R.C. Rocha-Filho, S.R. Biaggio, Galvanostatic Pb(II) removal from a simulated wastewater by using a stainless steel wool cathode in a flow-through cell: a factorial-design study, J. Appl. Electrochem. 38 (2008) 167–173.
[3] C. Flox, P.L. Cabot, F. Centellas, J.A. Garrido, R.M. Rodríguez, C. Arias, E. Brillas, Solar photoelectro-Fenton degradation of cresols using a flow reactor with a boron-doped diamond anode, Appl. Catal. B: Environ. 75 (2007) 17–28.
[4] L.S. Andrade, T.T. Tasso, D.L. Silva, R.C. Rocha-Filho, N. Bocchi, S.R. Biaggio, On the performances of lead dioxide and boron-doped diamond electrodes in the anodic oxidation of simulated wastewater containing the Reactive Orange 16 dye, Electrochim. Acta 54 (2009) 2024–2030.
[5] E. Brillas, I. Sirés, M.A. Oturan, Electro-Fenton process and related electrochemical technologies based on Fenton's reaction chemistry, Chem. Rev. 109 (2009) 6570–6631.
[6] M. Panizza, G. Cerisola, Direct and mediated anodic oxidation of organic pollutants, Chem. Rev. 109 (2009) 6541–6569.
[7] Ch. Comninellis, G. Chen (Eds.), Electrochemistry for the Environment, Springer, New York, 2010.
[8] L.C. Almeida, S. Garcia-Segura, N. Bocchi, E. Brillas, Solar photoelectro-Fenton degradation of paracetamol using a flow plant with a Pt/air-diffusion cell coupled with a compound parabolic collector: process optimization by response surface methodology, Appl. Catal. B: Environ. 103 (2011) 21–30.
[9] E. Brillas, M.A. Baños, M. Skoumal, P.L. Cabot, J.A. Garrido, R.M. Rodríguez, Degradation of the herbicide 2,4-DP by anodic oxidation, electro-Fenton and photoelectro-Fenton using platinum and boron-doped diamond anodes, Chemosphere 68 (2007) 199–209.
[10] S. Irmak, H. Yavuz, I. Halil, O. Erbatur, Degradation of 4-chloro-2-methylphenol in aqueous solution by electro-Fenton and photoelectro-Fenton processes, Appl. Catal. B: Environ. 63 (2006) 243–248.
[11] M. Diagne, N. Oturan, M.A. Oturan, Removal of methyl parathion from water by electrochemically generated Fenton's reagent, Chemosphere 66 (2007) 841–848.
[12] I. Sirés, N. Oturan, M.A. Oturan, R.M. Rodríguez, J.A. Garrido, E. Brillas, Electro-Fenton degradation of antimicrobials triclosan and triclocarban, Electrochim. Acta 17 (2007) 5493–5503.
[13] S. Hammami, N. Oturan, N. Bellakhal, M. Dachraoui, M.A. Oturan, Oxidative degradation of direct Orange 61 by electro-Fenton process using a carbon felt electrode: application of the experimental design methodology, J. Electroanal. Chem. 610 (2007) 75–84.
[14] A. Özcan, Y. Şahin, K. Savaş, M.A. Oturan, Degradation of picloram by the electro-Fenton process, J. Hazard. Mater. 153 (2008) 718–727.
[15] B. Balci, N. Oturan, R. Cherrier, M.A. Oturan, Degradation of atrazine in aqueous medium by electrocatalytically generated hydroxyl radicals. A kinetic and mechanistic study, Water Res. 43 (2009) 1924–1934.
[16] A. Dhaouadi, N. Adhoum, Degradation of paraquat herbicide by electrochemical advanced oxidation methods, J. Electroanal. Chem. 637 (2009) 33–42.
[17] M.A. Oturan, M.C. Edelahi, N. Oturan, K. El Kacemi, J.J. Aaron, Kinetics of oxidative degradation/mineralization pathways of the phenylurea herbicides diuron, monuron and fenuron in water during application of the electro-Fenton process, Appl. Catal. B: Environ. 97 (2010) 82–89.
[18] A. Wang, J. Qu, H. Liu, J. Ru, Mineralization of an azo dye Acid Red 14 by photoelectro-Fenton process using an activated carbon fiber cathode, Appl. Catal. B: Environ. 84 (2008) 393–399.
[19] E. Brillas, B. Boye, M.M. Dieng, General and UV-assisted cathodic Fenton treatments for the mineralization of the herbicide MCPA, J. Electrochem. Soc. 150 (2003) E583–E589.
[20] M. Zarei, A.R. Khataee, R. Ordikhani-Seyedlar, M. Fathinia, Photoelectro-Fenton combined with photocatalytic process for degradation of an azo dye using supported TiO_2 nanoparticles and carbon nanotube cathode: neural network modeling, Electrochim. Acta 55 (2010) 7259–7265.
[21] A.R. Khataee, M. Zarei, L. Moradkhannejhad, Application of response surface methodology for optimization of azo dye removal by oxalate catalyzed photoelectro-Fenton process using carbon nanotube-PTFE cathode, Desalination 258 (2010) 112–119.
[22] M. Zarei, A. Niaei, D. Salari, A. Khataee, Application of response surface methodology for optimization of peroxi-coagulation of textile dye solution using carbon nanotube-PTFE cathode, J. Hazard. Mater. 173 (2010) 544–551.
[23] K. Cruz-Gonzalez, O. Torres-Lopez, A. Garcia-Leon, J.L. Guzman-Mar, L.H. Reyes, A. Hernandez-Ramirez, J.M. Peralta-Hernandez, Determination of optimum operating parameters for Acid Yellow 36 decolorization by electro-Fenton process using BDD cathode, Chem. Eng. J. 160 (2010) 199–206.
[24] Y. Sun, J.J. Pignatello, Photochemical reactions involved in the total mineralization of 2,4-D by iron(3+)/hydrogen peroxide/UV, Environ. Sci. Technol. 27 (1993) 304–310.
[25] C.A. Martinez-Huitle, S. Ferro, Electrochemical oxidation of organic pollutants for the wastewater treatment: direct and indirect processes, Chem. Soc. Rev. 35 (2006) 1324–1340.
[26] I. Sirés, F. Centellas, J.A. Garrido, R.M. Rodríguez, C. Arias, P.L. Cabot, E. Brillas, Mineralization of clofibric acid by electrochemical advanced oxidation processes using a boron-doped diamond anode and Fe^{2+} and UVA light as catalysts, Appl. Catal. B: Environ. 72 (2007) 373–381.
[27] B. Boye, E. Brillas, B. Marselli, P.A. Michaud, Ch. Comninellis, G. Farnia, G. Sandonà, Electrochemical incineration of chloromethylphenoxy herbicides in acid medium by anodic oxidation with boron-doped diamond electrode, Electrochim. Acta 51 (2006) 2872–2880.
[28] E. Brillas, S. Garcia-Segura, M. Skoumal, C. Arias, Electrochemical incineration of diclofenac in neutral aqueous medium by anodic oxidation using Pt and boron-doped diamond anodes, Chemosphere 79 (2010) 605–612.
[29] Y. Zuo, J. Hoigné, Formation of hydrogen peroxide and depletion of oxalic acid in atmospheric water by photolysis of iron(III)–oxalato complexes, Environ. Sci. Technol. 26 (1992) 1014–1022.
[30] E. Guinea, F. Centellas, J.A. Garrido, R.M. Rodríguez, C. Arias, P.L. Cabot, E. Brillas, Solar photoassisted anodic oxidation of carboxylic acids in presence of Fe^{3+} using a boron-doped diamond electrode, Appl. Catal. B: Environ. 89 (2009) 459–468.
[31] A. Safarzadeh-Amiri, J.R. Bolton, S.R. Cater, Ferrioxalate-mediated solar degradation of organic contaminants in water, Sol. Energy 56 (1996) 439–443.
[32] J.M. Chacon, M.T. Leal, M. Sanchez, E.R. Bandala, Solar photocatalytic degradation of azo-dyes by photo-Fenton process, Dyes Pigments 69 (2006) 144–150.
[33] E.J. Ruiz, C. Arias, E. Brillas, A. Hernández-Ramírez, J.M. Peralta-Hernández, Mineralization of Acid Yellow 36 azo dye by electro-Fenton and solar photoelectro-Fenton processes with a boron-doped diamond anode, Chemosphere 82 (2011) 495–501.
[34] M.G. Cabral, C.A. Viegas, M.C. Teixeira, I. Sá-Correia, Toxicity of chlorinated phenoxyacetic acid herbicides in the experimental eukaryotic model *Saccharomyces cerevisiae*: role of pH and of growth phase and size of the yeast cell population, Chemosphere 51 (2003) 47–54.
[35] D.B. Donald, A.J. Cessna, E. Sverko, N.E. Glozier, Pesticides in surface drinking water supplies of the northern Great Plains, Environ. Health Perspect. 115 (2007) 1183–1191.
[36] T. Henriksen, B. Svensmark, B. Lindhart, R.K. Juhler, Analysis of acidic pesticides using in situ derivatization with alkylchloroformate and solid-phase microextraction (SPME) for GC–MS, Chemosphere 44 (2001) 1531–1539.
[37] A. Iglesias, R. López, D. Gondar, J. Antelo, S. Fiol, F. Arce, Adsorption of MCPA on goethite and humic acid-coated goethite, Chemosphere 78 (2010) 1403–1408.
[38] R.H. Myers, D.C. Montgomery, Response Surface Methodology, Wiley, New York, 2002.
[39] M.A. Bezerra, R.E. Santelli, E.P. Oliveira, L.S. Villar, L.A. Escaleira, Response surface methodology (RSM) as a tool for optimization in analytical chemistry, Talanta 76 (2008) 965–977.
[40] I. Grcicǐ, D. Vujevicǐ, J. Sepcicǐ, N. Koprivanac, Minimization of organic content in simulated industrial wastewater by Fenton type processes: a case study, J. Hazard. Mater. 170 (2009) 954–961.
[41] T.T.H. Pham, S.K. Brar, R.D. Tyagi, R.Y. Surampalli, Optimization of Fenton oxidation pre-treatment for *B. thuringiensis*-based production of value added products from wastewater sludge, J. Environ. Manage. 91 (2010) 1657–1664.
[42] O. Rozas, D. Contreras, M.A. Mondaca, M. Pérez-Moya, H.D. Mansilla, Experimental design of Fenton and photo-Fenton reactions for the treatment of ampicillin solutions, J. Hazard. Mater. 177 (2010) 1025–1030.
[43] F. Ay, E.C. Catalkaya, F. Kargi, A statistical experiment design approach for advanced oxidation of Direct Red azo-dye by photo-Fenton treatment, J. Hazard. Mater. 162 (2009) 230–236.
[44] A.G. Trovó, W.C. Paterlini, R.F.P. Nogueira, Evaluation of the influences of solution path length and additives concentrations on the solar photo-Fenton degradation of 4-chlorophenol using multivariate analysis, J. Hazard. Mater. B137 (2006) 1577–1582.
[45] A. Duran, J.M. Monteagudo, E. Amores, Solar photo-Fenton degradation of Reactive Blue 4 in a CPC reactor, Appl. Catal. B: Environ. 80 (2008) 42–50.
[46] A. Zapata, I. Oller, E. Bizani, J.A. Sánchez-Pérez, M.I. Maldonado, S. Malato, Evaluation of operational parameters involved in solar photo-Fenton degradation of a commercial pesticide mixture, Catal. Today 144 (2009) 94–99.
[47] J.M. Monteagudo, A. Duran, I. San Martin, M. Aguirre, Catalytic degradation of Orange II in a ferrioxalate-assisted photo-Fenton process using a combined UV-A/C–solar pilot-plant system, Appl. Catal. B: Environ. 95 (2010) 120–129.
[48] J. Virkutyte, E. Rokhina, V. Jegatheesan, Optimization of electro-Fenton denitrification of a model wastewater using a response surface methodology, Bioresour. Technol. 101 (2010) 1440–1446.

[49] S. Mohajeri, H.A. Aziz, M.H. Isa, M.A. Zahed, M.N. Adlan, Statistical optimization of process parameters for landfill leachate treatment using electro-Fenton technique, J. Hazard. Mater. 176 (2010) 749–758.
[50] G.E.P. Box, N.R. Draper, Empirical Model – Building and Response Surfaces, Wiley, New York, 1987.
[51] R.E. Bruns, I.S. Scarminio, B.B. Neto, Statistical Design – Chemometrics, Elsevier, Amsterdam, 2006.
[52] H. Lee, M. Shoda, Removal of COD and color from livestock wastewater by the Fenton method, J. Hazard. Mater. 153 (2008) 1314–1319.
[53] F.J. Benitez, J.L. Acero, F.J. Real, S. Roman, Oxidation of MCPA and 2,4-D by UV radiation, ozone, and the combinations UV/H_2O_2 and O_3/H_2O_2, J. Environ. Sci. Health B 39 (2005) 393–409.